



Published in final edited form as:

Neuron. 2019 September 04; 103(5): 853–864.e4. doi:10.1016/j.neuron.2019.06.003.

Non-Canonical Wnt-Signaling through *Ryk* Regulates the Generation of Somatostatin- and Parvalbumin-Expressing Cortical Interneurons

Melissa G. McKenzie^{1,2}, Lucy V. Cobbs², Patrick D. Dummer¹, Timothy J. Petros^{2,3}, Michael M. Halford⁴, Steven Stacker⁴, Yimin Zou⁵, Gord J. Fishell^{2,6}, Edmund Au^{1,2,7,8,*}

¹Department of Pathology and Cell Biology, Columbia University Medical Center, New York, NY 10032, USA

²NYU Neuroscience Institute, New York University Langone Medical Center, New York, NY 10016, USA

³Present Address: Eunice Kennedy-Shriver National Institutes of Child Health and Human Development, National Institutes of Health, Bethesda, MD 20892, USA

⁴Peter McCallum Cancer Center, University of Melbourne, Melbourne, Victoria 8006, Australia

⁵Neurobiology Section, Biological Sciences Division, University of California, San Diego, CA 92093, USA

⁶Department of Neurobiology, Harvard Medical School, Boston, MA 04115 and the Stanley center at the Broad, Cambridge, MA 02142

⁷Department of Rehabilitation and Regenerative Medicine, Columbia University Medical Center, New York, NY 10032, USA

⁸Columbia Translational Neuroscience Initiative Scholar, Columbia University Medical Center, New York, NY 10032, USA

Summary

GABAergic interneurons have many important functions in cortical circuitry, a reflection of their cell diversity. The developmental origins of this diversity are poorly understood. Here, we identify rostral-caudal regionality in Wnt exposure within the interneuron progenitor zone delineating the specification of the two main interneuron subclasses. Caudally-situated medial ganglionic

*Correspondence: ea2515@cumc.columbia.edu (Lead Contact).

Author Contributions

M.G.M. conducted and analyzed the majority of experiments. L.V.C. conducted analysis of *Ryk* ICD gain-of-function experiments. P.D.D. performed western blots. T.J.P. conducted electroporation experiments. M.M.H. and S.S. assisted with *Ryk* ICD constructs, *Ryk* function-blocking antibody and *Ryk* null mouse. Y.Z. contributed *Ryk* conditional mouse. G.J.F. contributed to experimental design. E.A. and M.G.M. designed experiments and co-wrote manuscript. E.A. conceived of study.

Publisher's Disclaimer: This is a PDF file of an unedited manuscript that has been accepted for publication. As a service to our customers we are providing this early version of the manuscript. The manuscript will undergo copyediting, typesetting, and review of the resulting proof before it is published in its final citable form. Please note that during the production process errors may be discovered which could affect the content, and all legal disclaimers that apply to the journal pertain.

Declaration of Interests:

The authors declare no competing interests.

eminence (MGE) progenitors receive high levels of Wnt signaling and give rise to somatostatin (SST)-expressing cortical interneurons. Parvalbumin (PV)-expressing basket cells, by contrast, originate mostly from the rostral MGE where Wnt signaling is attenuated. Interestingly, rather than canonical signaling through β -catenin, signaling via the non-canonical Wnt receptor Ryk regulates interneuron cell-fate specification *in vivo* and *in vitro*. Indeed, gain-of-function of Ryk intracellular domain signaling regulates SST and PV fate in a dose-dependent manner, suggesting Ryk signaling acts in a graded fashion. These data reveal an important role for non-canonical Wnt-Ryk signaling in establishing the correct ratios of cortical interneuron subtypes.

eTOC

Non-canonical Wnt signaling through the Ryk receptor establishes regional subdomains within the MGE along the rostral-caudal axis. These subdomains are defined by graded Ryk signaling, which regulates the proportions of parvalbumin and somatostatin cortical interneurons produced during development.

Introduction

Interneurons provide inhibitory tone and play critical roles in brain function: regulating cortical rhythmicity, attention states, and signal timing (Cardin et al., 2009; Fino and Yuste, 2011; Kvitsiani et al., 2013; Lapray et al., 2012). The majority of interneurons are contained within one of two broad cardinal classes: parvalbumin- (PV) and somatostatin- (SST) expressing cell types, which are fundamentally distinct in terms of their connectivity and contribution to brain function (Fishell and Rudy, 2011). The former are perisomal or axonal targeting, fast spiking and show synaptic depression (Hu et al., 2014; Inan et al., 2013; Taniguchi et al., 2013), whereas the latter provide inhibition to dendrites, are regular spiking and typically display synaptic facilitation (Lovett-Barron et al., 2012). Despite these differences, PV+ and SST+ interneurons originate from the same embryonic structure, the medial ganglionic eminence (MGE).

Understanding how functionally distinct cell types arise from a common origin remains a fundamental challenge. We have previously proposed that this process is essentially accomplished in two phases, *cardinal specification* into major subclasses followed by *definitive specification* of mature functional properties as they integrate into cortical circuitry (Kepecs and Fishell, 2014; Wamsley and Fishell, 2017). With respect to definitive specification, significant progress has been made in identifying extrinsic and intrinsic factors which act coordinately with neuronal activity to differentially fine-tune granular properties of interneurons (De Marco Garcia et al., 2011; De Marco Garcia et al., 2015; Dehorter et al., 2015). Furthermore, intrinsic regulation of interneuron identity by transcriptional regulation has been extensively studied (Wonders and Anderson, 2006). However, a conclusive extrinsic mechanism underlying cardinal specification is presently lacking. Previous findings have implicated multiple secreted growth factors, notably Shh, and key transcription factors for both the initial acquisition and later maintenance of cardinal identity (Anderson et al., 1997; Sussel et al., 1999; Tyson et al., 2015; Xu et al., 2010). Furthermore, there is evidence of spatial heterogeneity in the types of interneurons generated from different regions of the MGE (Flames et al., 2007; Hu et al., 2017; Wonders et al., 2008, Hu et al, 2017). Moreover,

during development, the proportion of subtypes produced shifts; SST+ cells are preferentially generated earlier, with the production of PV+ cells predominating at later developmental time points (Inan et al., 2012; Miyoshi et al., 2007). Therefore, a model to explain the precise orchestration of PV+ versus SST+ cardinal specification must: 1) account for the bias in spatial origins between the two subtypes, 2) cleanly delineate between PV+ and SST+, as well as 3) explain the proportional shift in subtype production over time.

Here we describe regional variability in Wnt-responsiveness along the caudal-rostral axis of the MGE that reflects Wnt sources emanating from caudally situated embryonic structures. Transplants of MGE subdomains along this axis reveal a strong bias in the spatial origin of PV+ and SST+ cells such that strongly Wnt-responsive cells become SST+ interneurons and lower levels of Wnt produce PV+ cells. We demonstrate that Ryk signaling is at least partially responsible for the delineation between PV+ and SST+ cell fate, independent of canonical Wnt signaling through β -catenin or Shh signaling. Genetic ablation of *Ryk* compromises the ability of nearly half of cells to acquire PV+ and SST+ interneuron identity; the remaining cells no longer exhibit a population bias for PV+ over SST+. We further show that Ryk signaling is dynamically regulated throughout development and parallels the differential production of SST+ and PV+ interneurons over time. Indeed, the proportion of SST+ and PV+ interneurons can be regulated in an *in vitro* model of interneuron development (Au et al., 2013) by directly modulating Ryk signaling. Therefore, Ryk signaling is a critical component of interneuron cardinal specification that controls the relative proportions of PV+ and SST+ subtypes produced and thus enables proper microcircuit assembly.

Results

Previous work has shown that the initial specification of interneuron subtype identity is determined at the progenitor phase, prior to the exit from the cell cycle (Butt et al., 2005; Inan et al., 2012; Nery et al., 2002; Taniguchi et al., 2013; Wichterle et al., 2001). In a variety of developmental contexts, morphogen gradients have been shown to create variation and diversity within progenitor fields, a process most thoroughly studied with regard to sonic hedgehog signaling in the spinal cord (Briscoe and Ericson, 2001; Dessaud et al., 2007; Ericson et al., 1997; Roelink et al., 1995). Similarly, a number of studies have indicated that sonic hedgehog signaling within the MGE also biases interneuron subtype identity (Flames et al., 2007; Inan et al., 2013; Puelles and Rubenstein, 2003; Rubenstein et al., 1994; Taniguchi et al., 2013; Wonders et al., 2008). However, a role for other morphogens in the production of PV+ or SST+ cells from the MGE remains elusive.

Expression of Wnt signaling components suggests a caudal to rostral gradient across the MGE

Wnt has been found to play an important role in the expansion of the subventricular zone within the MGE (Gulacsi and Anderson, 2008) and the PV+ interneurons that preferentially arise from this proliferative area (Glickstein et al., 2007; Gulacsi and Anderson, 2008; Petros et al., 2015). This led us to investigate whether Wnt might play additional roles in patterning the MGE by providing graded signaling, as has been described elsewhere in the nervous

system (Charron and Tessier-Lavigne, 2005; Lee and Jessell, 1999). Using publically available CNS gene expression data from the Allen Institute, we performed an *in silico* screen and found that multiple Wnt ligands are expressed in close proximity to the MGE (Supplemental Figure 1, Figure 1) (Website: ©2013 Allen Institute for Brain Science. Allen Developing Mouse Brain Atlas [Internet]. Available from: <http://developingmouse.brain-map.org>). Caudal to the MGE, *Wnt7a* and *Wnt7b* are both highly expressed in the superficial stratum of the prethalamic eminence as well as in the cortical hem (Figure 1D, Supplemental Figure 1), where *Wnt3a* and *Wnt5a* are also expressed (Supplemental Figure 1). TCF7L2, a canonical Wnt-responsive transcription factor is also present in the caudal aspect of the MGE mantle, where newborn interneurons begin their migration (Figure 1E). A Wnt reporter mouse expressing a destabilized histone 2B-eGFP fusion protein under the control of general TCF/LEF promoter elements (Ferrer-Vaquer et al., 2010) (*Wnt reporter*) also shows enriched eGFP expression in the caudal aspect of the MGE, suggestive of a caudal-high, rostral-low Wnt gradient of responsiveness within the MGE (Figure 1F, 3A). Within the rostral aspect of the MGE, the Wnt antagonist *Sfrp1* (Secreted frizzled receptor protein 1) is expressed (Supplemental Figure 2). Upon further investigation of genes with similar enrichment in the MGE to *Nkx2-1*, we discovered that a large number of genes display a caudal-rostral divergence in their expression pattern (Supplemental Figure 2). We therefore hypothesized that this regionality may arise from differences in exposure to Wnt ligands, resulting in signaling gradients that underlie previously described regional variation in generation of interneuron cell types (Wonders et al., 2008, Flames et al, 2007, Hu et al, 2017).

The rostral and caudal MGE give rise to different interneuron subclasses

Our lab has previously employed ultrasound backscatter microscopy (UBM) as a means of grafting donor ventral eminence tissue into specific substructures of host embryonic brain. Through such fate mapping we demonstrated that donor eGFP+ MGE cells, when transplanted into wildtype recipient host MGE, migrate dorsally and integrate throughout the cortex alongside endogenous interneurons (Butt et al., 2005; Nery et al., 2002; Wichterle et al., 2001). To directly examine whether rostral vs. caudal MGE (rMGE and cMGE, respectively) -derived cortical interneurons assume different fates within the cortex, we used a similar UBM transplantation approach (Figure 2). From embryos ubiquitously expressing TdTomato, the caudal (high Wnt) and rostral (low Wnt) portions of e12.5 embryonic MGEs were microdissected and transplanted into the MGE of e13.5 unlabeled host embryos (Figures 2A and B, Supplemental Figure 3). Brains from animals receiving grafts were collected at postnatal day 21 (p21) when interneuron progenitors have fully matured. Transplanted cells were scored for expression of SST or PV by immunohistochemistry (Figure 2C). Compared to control transplants of the whole MGE (wMGE), rMGE and cMGE transplants were strongly biased for PV and SST, respectively (wMGE n=8 63% PV, 37% SST of identified cells, std. dev 4.5%, 25% unidentified of all labeled cells, rMGE n=14 71% PV, 29% SST of identified cells, 29% unidentified of all labeled cells, std dev 7.3%, cMGE n=4 16% PV, 84% SST of identified cells, std dev 2.4%, 23% unidentified of all labeled cells, chi-squared test p value=.02, 0.0001, Figure 2D).

Fate-mapped Wnt-responsive cells are biased toward production of SST+ interneurons

Since the presence of SST+ cells was strikingly enriched in the cMGE, we sought to establish a more direct relationship between Wnt-responsiveness in MGE progenitors and SST+ cell fate. To do so, we made use of the histone 2B-eGFP *Wnt reporter* mouse mentioned above (Figure 1F, 3A) (Ferrer-Vaquer et al., 2010). In order to both identify cells that receive strong Wnt signaling at e12.5 and characterize them as they achieve their mature fate, we crossed the Wnt reporter onto a background ubiquitously expressing tdTomato. We then dissected MGEs from e12.5 embryos and used flow cytometry to capture cells with high levels of nuclear eGFP expression, indicating high levels of Wnt signaling activity (Figure 3C, green box and Supplemental Figure 3). After transplanting flow cytometry-isolated nuclear eGFP+ cells into unlabeled hosts, transplanted cells, marked by their expression of tdTomato, were scored for marker expression at p21. Overwhelmingly, embryonic progenitors with high levels of Wnt activity gave rise to SST+ cells (Figure 3D) (9% PV+, 91% SST+, of identified cells, 18% Unidentified cells of total reporter labeled cells, n=2, compared to wMGE p=.0003, student's unpaired t-test).

Wnt inhibition decreases SST+ interneuron production

In order to establish a causal link between Wnt signaling and interneuron identity, we administered IWP2, a small molecule inhibitor of the membrane bound O-acyl transferase (MBOAT) protein, Porcupine (Porcn) (Chen et al., 2009). Porcupine is essential for the post-translational acylation and secretion of all secreted Wnts (Barrott et al., 2011; Proffitt and Virshup, 2012; Willert et al., 2003). Indeed, IWP2 injection into the ventricle of e12.5 *Wnt reporter* mice dramatically reduced Wnt reporter expression within 24 hours (Figure 3A, B). We hypothesized that a reduction in Wnt signaling would mimic an expansion of the low Wnt rostral MGE and result in a proportional decrease of SST+ cells. To test this, we injected the ventricles of fluorescently labeled mice with IWP2 at e12.5 and collected MGE tissue 24 hours later for transplantation into e13.5 host embryos (Figure 3A, red box). When we analyzed hosts at p21, we found a reduction in Wnt signaling resulted in a dramatic increase of interneurons that adopted a PV+ fate compared to wMGE transplants (Figure 3D) (79% PV+, 21% SST+, of identified cells, 27% unidentified cells of total reporter expressing cells, n=4 p=.03 student's unpaired t-test compared to wMGE).

Canonical Wnt signaling does not significantly influence cell fate

Canonical Wnt signaling requires the intracellular signaling molecule β -catenin. Under basal conditions, β -catenin is sequestered within the cytoplasm and targeted for degradation by GSK3- β . Binding of Wnt ligand to the Frizzled (FZD) family of Wnt receptors prevents β -catenin degradation, resulting in its accumulation and translocation to the nucleus where it initiates the expression of TCF/LEFs to modulate gene expression (reviewed in Willert and Nusse, 2012). Previous work suggests that loss of canonical Wnt signaling influences proliferation in the MGE (Gulacsi and Anderson, 2008). MGE specific knockout of *β -catenin* is late-embryonic lethal however, preventing assessment of the mature cell types produced from the mutant MGE. To circumvent this lethality and to determine whether disrupting Wnt signaling through *β -catenin* affects cell type specification in the MGE, we generated e12.5 MGE specific knockouts of *β -catenin* (Brault et al., 2001). This was

achieved by crossing a conditional β -catenin^{ff} allele onto the *Nkx2.1^{Cre}* driver line and a conditional GFP reporter (Sousa et al., 2009; Xu et al., 2008). Embryonic mutants were identified by a midline fusion defect in the ventral forebrain, a phenotype characteristic of β -catenin loss of function in the MGE and confirmed by DNA genotyping after transplantation. Mutant MGEs were collected, dissociated, and transplanted into embryonic hosts (Figure 3B, orange box). Interestingly, analysis of this population at p21 showed that the loss of β -catenin-signaling resulted in a non-significant trend towards SST+ cell production compared to wMGE (41% PV+, 56% SST+ of identified cells n=3, p=0.1 paired student's t-test compared to wMGE, 25% unidentified). The opposing effect between β -catenin loss and Wnt inhibition lead us to consider the role of non-canonical Wnt signaling pathways.

Non-Canonical Wnt receptor, Ryk is preferentially active in cMGE

Wnt signals through a number of β -catenin-independent pathways, including the planar cell polarity and convergent extension pathways, as well as non-FZD receptors including Ryk, Ror1, and Ror2 (Green et al., 2014). To identify the most promising candidates mediating non-canonical Wnt signaling within the MGE, we measured the expression levels of a number of non-canonical Wnt signaling genes in e13.5 MGE by RT-PCR. Many non-canonical Wnt signaling components were expressed at negligible levels; the exceptions being *Vangl2*, a membrane protein important for the planar cell polarity pathway and Ryk, a receptor-like tyrosine kinase that binds Wnt (Figure 4A). Forebrain-specific knockouts of *Vangl2* are viable throughout adulthood and display no phenotypes suggestive of MGE interneuron deficits such as seizures (Qu et al., 2014; A. Goffinet personal communication). By contrast, Ryk has been shown to have a role in cortical neurogenesis and in MGE cell production; *Ryk*^{-/-} animals are perinatal lethal, which has precluded analysis of which interneuron subtypes are affected (Lyu et al., 2008; Zhong et al., 2011).

Ryk signaling in cortical neurogenesis occurs via the cleavage and nuclear translocation of the intracellular portion of the Ryk receptor (Lyu et al., 2008). Cleavage of the Ryk receptor by γ -secretase is constitutive and independent of Wnt signaling (Lyu et al., 2008). Through an unknown mechanism, the presence of Wnt ligand is thought to induce the translocation of the cleaved Ryk intracellular domain (Ryk ICD) from the cytoplasm to the nucleus (Lyu et al., 2008). In order to establish whether Ryk signaling was differentially active in the rMGE vs. cMGE, we compared protein from pooled samples of rostral and caudal MGE (Figure 4B). We fractionated protein samples from the rostral, caudal and whole MGE into whole cell, cytoplasmic, and nuclear fractions, and assessed Ryk activation by Ryk ICD levels in the nucleus. By western blot, we found Ryk ICD to be enriched in the nuclear fraction of the cMGE compared to the rMGE (Figures 4C and E), indicating that Ryk receptor activation aligns with the predicted regionality of Wnt exposure. Our previous experiments indicated that inhibition of Wnt by IWP2 treatment both significantly decreases the amount of canonical Wnt signaling by the TCF/LEF eGFP reporter activation and the number of SST+ interneurons produced (Figure 3B, D). Consistent with prior reports that Ryk ICD signaling (Lyu et al, 2008) is modulated by Wnt, we found that MGEs treated with the Wnt inhibitor IWP2 for 24 hours showed a significant decrease in Ryk ICD signal in the cytoplasmic

fraction compared with vehicle treated controls (Figure 4D, G). Full-length Ryk receptor signal was also decreased in IWP2 treated MGE samples (Figure 4F).

During development, the proportions of PV+ and SST+ interneurons produced by the MGE change. While SST+ interneurons are strongly enriched in early cohorts, the production of PV+ interneurons predominates during later stages of embryonic development. We therefore examined presence of nuclear Ryk ICD in wMGE across developmental ages (e11.5 to e15.5). We observed a peak of nuclear Ryk ICD at e12.5 that declined at later ages (Figure 4H), consistent with the dynamic output of SST+ and PV+ interneurons over time. Furthermore, *in situ* hybridization of Ryk shows a decline in expression in the MGE with developmental age (Figure 4J). Wnt 7a and 7b expression in the thalamus and hem also decline at later stages (Supplemental Figure 1). (Website: ©2013 Allen Institute for Brain Science. Allen Developing Mouse Brain Atlas [Internet]. Available from: <http://developingmouse.brain-map.org>.) These data demonstrate that Wnt ligands, Ryk expression, and the presence of nuclear Ryk ICD all decline during periods of reduced SST+ interneuron production and are consistent with the hypothesis that they are coordinately regulated.

Ryk signaling regulates SST+ and PV+ generation embryonically

We observed Ryk ICD signaling to be enriched in the caudal MGE, coincident with SST+ interneuron production. To test the sufficiency of activating Ryk signaling in SST fate specification, we utilized a previously employed Ryk gain-of-function strategy (Lyu et al., 2008). To do so, we generated a Cre recombinase-dependent plasmid expressing the intracellular portion of the Ryk receptor tethered to a nuclear localization signal, as has been used previously to mimic constitutive Wnt-independent Ryk activation (nls-Ryk ICD) (Lyu et al., 2008). Electroporation of this plasmid into the MGE of *Nkx2.1^{Cre}* embryos at e12 resulted in a significant increase in the number of SST+ cells (compared to electroporation of control plasmid) produced in the electroporated cohort when assessed at p21 (Figure 5A). A concomitant decrease in the amount of PV+ interneurons in these same experiments was also observed (Figure 5A, *RICD* n=3, Control n=3, chi-squared test $p < .0001$).

A previous study examining *Ryk^{-/-}* embryos observed decreased MGE interneuron production and an increase in oligodendrogenesis (Zhong et al., 2011). However, the perinatal lethality of null animals prevented mature cortical interneuron subtype analysis. To circumvent this issue, we engrafted *Ryk^{-/-}* MGE tissue into wildtype hosts to determine whether loss of *Ryk* affects the fate of interneurons in these mutants (Figure 5B). Ubiquitous TdTomato+;*Ryk^{+/-}* animals were crossed and at e12.5, *Ryk^{-/-}* embryos were identified for dissection by PCR genotyping (see methods). Fluorescently labeled mutant MGEs were then transplanted into wild-type e13.5 host embryos for postnatal analysis. *Ryk^{-/-}* transplants were capable of robust migration and integration into host cortex (Supplemental Figure 4), but interestingly, the majority of *Ryk^{-/-}* interneurons failed to fully differentiate as evidenced by the lack of mature cIN subtype marker expression, including CGE interneuron markers (Figure 5B) (50% unidentified, n=2).

Eliminating *Ryk* entirely in the brain throughout development clearly has a marked effect on interneuron specification and production. As such, we wished to more precisely block Ryk function during a more restricted time window in order to examine the role of Ryk in PV+

and SST+ interneuron specification. To do so, we introduced a Ryk extracellular domain human function-blocking antibody (Halford et al., 2013) into the ventricles of e12 embryos. When analyzed at p21, animals treated with a Ryk function blocking antibody had normal numbers of MGE derived interneurons in the cortex, but showed a ~15% increase in PV complemented by a ~15% decrease in SST numbers in the cortex, suggesting that Ryk blockade induced a fate switch (n=4, student's unpaired t-test p=0.03 Supplemental Figure 5).

Finally, in order to genetically ablate *Ryk* without perinatal lethality, we conditionally removed Ryk in the MGE while fate mapping the resulting mutant cells: *Nkx2-1^{Cre}; Ai9; Ryk^{f/f}* with *Nkx2-1^{Cre}; Ai9; Ryk^{f/+}* mice used as controls. At postnatal day 21, nearly half (41.3%) of tdTomato+ cells did not express PV or SST (Figure 5C, Supplemental Figure 5), oligodendrocyte, or CGE interneuron subtype markers (Supplemental figure 6). Moreover, of the remaining tdTomato+ cells that expressed PV and SST (49.6% PV and 50.3% SST), there was no longer a population bias whereas in controls, PV+ cells outnumbered SST+ cells (65.1% PV and 34.8% SST) (Figure 5C, Supplemental Figure 6, controls n=4, mutants n=3, p= <.0001, chi-squared test). The dramatic increase in unidentified cells raises the intriguing possibility that Ryk signaling is important for the maturation of interneurons. Post-mitotic removal of Ryk from SST populations with *SST^{Cre}* or broadly using the post-mitotic interneuron driver *Dlx6a^{Cre}*, however, resulted in no changes in interneuron marker expression (Supplemental figure 5). Taken together, these data strongly suggest that Ryk signaling regulates the generation of both PV+ and SST+ interneurons during the progenitor phase.

The reduction, but not complete loss, of PV and SST interneuron subtype markers when Ryk signaling is removed in MGE progenitors suggests alternate or redundant mechanisms to achieve interneuron subtype fate decisions. Sonic hedgehog signaling has previously been implicated in regional variation of interneuron production from the MGE, leading to the question as to whether Ryk and Shh pathways interact. To test if Shh acts in parallel or in series with Ryk signaling, we injected the Shh antagonist cyclopamine into the ventricle of e12.5 *Nkx2.1^{Cre}; Ryk^{f/+}* and *Ryk^{f/fl}* embryos. We reasoned that if Shh is an alternative or redundant mechanism for MGE cell specification that Shh blockade would result in an exacerbation of the Ryk mutant phenotype, perhaps leading to an increase in the number of unidentified (PV-, SST-) cells. Analysis at e13.5 revealed that cyclopamine treatment resulted in a decrease in expression of the Shh-responsive transcription factor Gli1 (Supplemental figure 5) in the MGE. However, P21 analysis of cyclopamine-treated animals did not demonstrate significant changes in PV+ or SST+ interneurons numbers in the cortex of treated mutants or controls (Figure 5D).

Graded Ryk activation regulates the production of SST+ and PV+ interneurons from embryonic stem cells

Data from *Ryk^{-/-}* transplants, Ryk conditional loss of function, and Ryk ICD gain of function experiments, suggest Ryk ICD signaling drives SST+ and is required for PV+ interneuron production. We observed high levels of nuclear Ryk ICD in the cMGE, and low, but detectable Ryk ICD in the rostral MGE. We also noted a gradual decrease in Ryk

signaling in the MGE developmentally (Figure 4E). Taken together, these data suggest Ryk acts in a graded, dose-dependent manner, where high Ryk signaling favors the production of SST⁺ interneurons, and low Ryk signaling favors the production of PV⁺ interneurons. To directly test this hypothesis, we made use of an *in vitro* gain-of-function model system we previously devised whereby mouse ES cells are transcriptionally specified to become cortical interneurons (Figure 6A) (Au et al., 2013). In the context of this system, we introduced a constitutively active form of Ryk ICD (nls-Ryk ICD) element described above, is under the control of a doxycycline-repressible TET element, tTA^{2S}. This allows us to titer the levels of expression of activated Ryk by varying the concentration of doxycycline introduced in culture during differentiation (Figure 6B, see methods). Previous work from our lab has shown that cortical interneurons derived from this system develop normally *in vivo* (Au et al., 2013). When transplanted into the MGE of an embryonic host, they migrate, integrate and mature in a manner indistinguishable from their endogenous counterparts. This allows for the postnatal *in vivo* analysis of mature ES cell-derived interneurons. In the absence of doxycycline, nls-Ryk ICD is expressed at maximum levels. This resulted in virtually all ES-derived interneurons adopting an SST⁺ identity (91% SST⁺, 9% PV⁺, n=4). The addition of a low concentration of doxycycline partially depressed the levels of induced nls-Ryk ICD and resulted in an increased number of PV⁺ cortical interneurons being produced (50% SST⁺, 50% PV⁺, n=3, p=0.001, paired student's t-test compared with no doxycycline condition). Higher levels of doxycycline further decreased nls-Ryk ICD levels and resulted in the production of proportionally more PV⁺ interneurons and fewer SST⁺ cells (34% SST⁺, 66% PV⁺, n=4, p=0.03, paired student's t-test compared with no doxycycline condition) (Figure 6C). These data indicate that Ryk signaling influences the proportion of PV⁺ versus SST⁺ interneurons on a population level by controlling the amount of SST⁺ interneurons produced in a graded fashion.

Discussion

In this study, we describe a caudal to rostral axis in Wnt-responsiveness within the MGE. The production of SST⁺ and PV⁺ cortical interneurons parallels this axis: SST⁺ cells originate in the caudal MGE in close proximity to Wnt, and PV⁺ cells arise from the rostral MGE distal to the Wnt source. We find that Wnt-responsive cells from the MGE overwhelmingly become SST⁺ interneurons and that Wnt is required for a population bias in cIN identity. We further demonstrate that the non-canonical Wnt receptor Ryk plays an active role in specifying SST⁺ fate through its intracellular domain. Activation of the Ryk pathway in MGE progenitors biases cells towards SST⁺ identity. Importantly, MGE-specific genetic loss of *Ryk* function results in a large proportion of both PV⁺ and SST⁺ cells failing to acquire subtype identity. Together, these data suggest that while high levels of Ryk signaling drive the normal generation of SST⁺ interneurons, low levels of Ryk signaling are required for the generation of a large proportion of PV⁺ interneurons. Consistent with this notion, we demonstrate that graded levels of Ryk signaling, through nuclear localization of Ryk ICD, regulate the proportions of SST⁺ and PV⁺ cINs produced from an ES cell-based model system of interneuron development. These data strongly suggest that Ryk signaling is a key component in mediating interneuron subclass specification and acts in a graded

fashion to regulate the proportions of interneuron subclasses produced over developmental time.

Our findings are in accordance with observed differences of gene expression across spatial subdomains of the MGE (Flames et al., 2007). Previous studies also indicate spatial biases in the cell types produced in different MGE subdomains (Wonders et al., 2008; Hu et al., 2017). These studies have largely focused on the dorsal-ventral axis along the MGE. For instance, findings from the Anderson laboratory have implicated Shh-signaling in regulating the specification of SST+ versus PV+ interneurons (Tyson et al., 2015; Xu et al., 2010; Xu et al., 2005). Recent work has also described rostral-caudal MGE transcription factor subdomains (Hu et al., 2017). For simplicity, we have referred to the regional variability described here as being oriented caudal to rostral. More precisely, it is based on progenitor cell proximity to Wnt, likely emanating from the thalamus, which is located dorsally and towards the caudal midline relative to the MGE. As such, our results are consistent with previous studies reporting SST+ interneurons and PV+ interneurons preferentially derived from dorsal MGE and ventral MGE, respectively (Wonders et al., 2008). In an attempt to reconcile the previously reported role of Shh signaling in interneuron subclass specification, we pharmacologically attenuated Shh by intraventricular cyclopamine injection at e12.5. While this resulted in a decrease in Gli1 expression in the MGE, it did not alter PV and SST numbers at P21 in Ryk wildtype animals. Further, it did not exacerbate the phenotype in Ryk mutants, where the number of unidentified cells was unaffected. These data suggest that Shh regulation of interneuron identity likely occurs prior to e12.5 when cyclopamine was administered. And critically, it also suggests that in the absence of Ryk signaling, Shh does not serve a redundant role to establish interneuron identity in the PV and SST cells that retain marker expression.

In the MGE, Wnt signaling appears to play multiple roles. While canonical Wnt signaling is critical for MGE expansion (Gulacsi and Anderson, 2008), we found that genetic ablation of β -catenin in the MGE results in little change in the relative proportion of different interneuron subtypes. Interestingly, these data suggest that Wnt proliferative and specification functions can be deconvolved, potentially along different signaling pathways. Importantly, canonical Wnt loss of function results in a trend of decreased PV+ interneurons, in accordance with studies suggesting that PV+ cell progenitors preferentially undergo transit amplification and thus are likely more sensitive to proliferative manipulations (Glickstein et al., 2007; Petros et al., 2015). Similarly, Ryk activity plays a role in directing the mode of neurogenesis adopted by cortical progenitors (Lyu et al., 2008). Therefore Shh, canonical Wnt, and non-canonical Wnt signaling may participate in both proliferation and patterning across developmental time scales. Loss of Shh signaling in MGE progenitors at e10.5 results in changes in interneuron production (Xu et al., 2010). By contrast, we have demonstrated that cyclopamine treatment at e12.5 does not significantly affect interneuron fate specification, suggesting that Shh morphogenic effects occur predominantly at earlier time points. Conversely, treatment of embryos at e12.5 with the Wnt inhibitor IWP2 results in a significant fate-switch in interneuron subclasses. Collectively, our data suggest that Wnt signaling shifts from a predominantly proliferative to a fate-determinative role over developmental time. Thus, there remains the intriguing possibility for overlap in the effects

of Wnt and Shh signaling as they impinge on the mode of neurogenesis and proliferation rates during early MGE patterning.

In addition to its role in regulating proliferation, Wnt is a well-known determinant of cell fate in both invertebrates and vertebrates. Within the nervous system, Wnt has an early role as a dorsalizing factor during early stages of development (reviewed in Lee and Jessell, 1999). The present findings indicate a later role for Wnt signaling in forebrain patterning, as a secondary gradient emanating from dorso-caudal signaling sources. Importantly, these data highlight the utility of considering the forebrain in three-dimensions, and the constantly evolving spatial relationship between neighboring structures. Much like the notochord induces the nearby floorplate in the developing spinal cord (Placzek et al., 2000), the gradient we describe here is a reflection of how spatially positioned co-developing structures are important sources of developmental signals.

Wnt-Ryk signaling via the planar cell polarity pathway has been previously implicated in neuronal development (Hollis et al., 2016; Lanoue et al., 2017; Macheda et al., 2012; Nusslein-Volhard and Wieschaus, 1980; Reynaud et al., 2015; Schmitt et al., 2006). A number of other studies have found that translocation of the Ryk intracellular domain to the nucleus in response to Wnt activity directs progenitor cell neurogenesis in the developing dorsal and ventral forebrain (Chang et al., 2017; Kamitori et al., 2005; Lyu et al., 2008; Zhong et al., 2011). Our findings also suggest that Ryk ICD signaling plays an important role in interneuron subtype identity. Conditional loss of function of Ryk in the MGE (*Nkx2.1^{Cre}; Ryk^{f/f}*) resulted in a dramatic decrease in specified interneurons and equal proportions of PV+ and SST+ cells, a pronounced departure from their normal 65:35 ratio. Notably, transplantation of *Ryk^{-/-}* MGE replicated our findings by genetic loss-of-function, bolstering the notion that MGE transplantation is a valid approach where conditional loss of function allele is unavailable.

Overall our loss of function analysis indicates that Ryk signaling is crucial for the specification of both PV+ and SST+ interneurons. Interestingly, Ryk loss-of-function progenitors are capable of generating specified cells, although without the normal ratio observed in wild-type interneurons. These data suggest the presence of redundant systems that allow for the production of PV+ and SST+ interneurons (albeit with many unspecified cells) in the absence of Ryk signaling. Importantly, we observed that PV and SST interneuron identity is not affected when Ryk is ablated postmitotically with either *Dlx6a^{Cre}* or *SST^{Cre}* driver lines. This indicates that the influence of Ryk signaling in subclass identity is confined to the MGE progenitor stage, consistent with previous findings (Butt et al, 2008)

We hypothesize that Ryk signaling stochastically biases nascent interneuron subtype identity as they become postmitotic. In this scenario, graded levels of Ryk signaling act to fine-tune and regulate MGE output in order to generate the appropriate numbers of PV+ and SST+ interneurons. We directly tested this hypothesis by using our previously established *in vitro* model system of interneuron development (Au et al., 2013). This enabled us to modulate the ratio of PV+/SST+ interneurons by varying the levels of Ryk ICD signaling in a doxycycline dose-dependent fashion. These data strongly support the idea that Ryk ICD signaling acts in a graded manner to determine cell fate decisions in the MGE.

Interneurons undergo a protracted period of development from the time of their generation to full maturity. The phenotypes observed in our analysis of conditional Ryk loss-of-function and grafting analysis of *Ryk*^{-/-} MGE suggest that in addition to playing a role in fate selection, *Ryk* may also contribute to interneuron maturation. In this study, we have limited our analysis to MGE neurogenesis. This is the period we have previously hypothesized is critical for cardinal specification of cell type. Subsequently, through a process we have termed definitive specification, interneuron fate is likely refined during both their migration and upon reaching their settling position (Kepecs and Fishell, 2014). Later aspects of interneuron maturation might also be influenced by the level of Ryk activity. Exploring these roles is an appealing area for future investigation. Higher throughput methods such as ES cell differentiation and transplantation may prove to be an effective approach to further study *Ryk*-dependent phenotypes in greater detail during these later phases. Regardless of its further roles, our findings indicate that Ryk signaling mediates morphogenetic signaling influencing the production of both PV+ and SST+ interneurons from MGE progenitor pools.

STAR Methods

Lead contact and Materials Availability

Further information and requests for resources and reagents should be directed to Edmund Au (ea2515@cumc.columbia.edu)

Experimental Model and Subject Details

Animal husbandry—All animal handling and maintenance were performed according to the regulations of the Institutional Animal Care and Use Committee of the NYU School of Medicine and Columbia University Medical center. The following lines were genotyped as previously described: *Nkx2-1^{Cre}* (Xu et al., 2008), *Ryk*^{-/-} (Halford et al., 2013) (RRID: MGI:2667559), *β-catenin^{fl/fl}* (Brault et al., 2001), *Tcf/Lef:H2B-dGFP* (Ferrer-Vaquer et al., 2010) (RRID: IMSR_JAX:013752), *Ai9* (Madisen et al., 2010) (equivalent: RRID: IMSR_JAX:007914), *RCE* (Sousa et al., 2009), and *TK^{Cre}* (Bai et al., 2002). *Ryk* conditional (Hollis et al., 2016) animals were received on a black 6 background (C57B6), mutant progeny were not initially observed when crossed onto *Nkx2.1^{Cre}* (also B6) homozygous mutant productive crosses occurred after outbreeding to the CD-1 background. Wild-type timed pregnant females for transplant recipients, IWP2 or Ryk function blocking antibody experiments were of the Swiss-webster background and ordered from Taconic. All embryonic time points were counted from discovery of vaginal plug (e0.5).

Cell culture—Mouse ES cells were maintained using standard protocols (Joyner, 2000). Low passage cell lines were differentiated using protocols described previously (Au et al., 2013; Watanabe et al., 2005). Briefly, ES cells in late log phase growth were dissociated into single cells and plated into non-TC treated wells at a density of 35 000 cells/well in order to establish floating embryoid body (EB) cultures. EBs were successively treated with Dkkopf-1 (2.5 ng/ml), and Sonic Hedgehog (40 ng/ml) for 11-13 days, after which they were gently dissociated (Accutase (Invitrogen), 15', 37°C) for subsequent experiments. The *RykICD* was generated by PCR using full length human *RYK* cDNA with a C-terminus myc tag (provided by Stephen Stacker, Peter MacCallum Cancer Centre, Melbourne, Australia)

as a template and cloning a nuclear localization signal in frame at the N-terminus (Lu et al., 2008). This construct was introduced into a bi-directional tet-responsive element driving Dlx2 in one direction and Ryk ICD in the other (Au et al., 2013). This assembly was then nucleofected into a *Dlx6a*^{Cre}; Ai9 reporter ES cell line along with Nestin-Nkx2-1-IRES-tTA (Lonza). Individual clones were isolated, expanded, genotyped and verified by *in vitro* differentiation.

Method Details

Protein Analysis—Tissue samples for protein analysis were dissected into rMGE, cMGE or wMGE fractions and processed as below. A minimum of 5 embryos were pooled for each embryonic sample condition. For cell culture protein analysis, embryoid bodies were collected at 11-13 days after differentiation, rinsed with PBS and resuspended in 100 µl of lysis buffer (95mM NaCl, 25mM Tris-HCl pH 7.5, 10mM EDTA and 2% SDS, final pH=8.0 including protease inhibitor mix (cOmplete Ultra Roche)), and homogenized with a brief pulse using an ultrasonicator with microtip (Misonix S-4000, amplitude=1, 5s pulse). Samples destined for fractionation were processed as described (Suzuki et al., 2010). Protein samples were quantified and lanes to be compared loaded with equal amounts of total protein. Blots were probed using an antibody mix and both channels imaged simultaneously with fluorescent secondary antibodies (Li-Cor). The following primary antibodies were used: Rabbit monoclonal anti Ryk N-term (AbCam, 1:50,000, [RRID:AB_10973565](#)), Rabbit anti-Ryk C-term (Thermo 1:1000, [RRID:AB_2285487](#)), Rabbit anti-Ryk N-term (Zou lab, 1:1000), mouse anti Cyclophilin A (Abcam 1µg/ml, [RRID:AB_879767](#)), Rb anti-histone H3 (Cell Signaling, 1:2000, [RRID:AB_331563](#)), mouse anti β-actin (1:2000). Blots were imaged using Odyssey CLx Infrared Imager and analyzed using ImageStudio software (LiCor). Protein fluorescent signal was normalized to beta actin loading control intensity in whole cell or cytoplasmic fractions, and to histone in nuclear fractions.

Immunohistochemistry—Embryos aged e15.5 or later and adult mice were transcardially perfused with 4% paraformaldehyde in PBS (4%PFA). Tissue was prepared for either cryosectioning and slide staining or vibratome sectioning followed by free-floating immunohistochemistry. Both cryosectioning and vibratome sectioning were used in transplantation experiments (Figures 2, 3, 5, 6). No difference was found between the two tissue preparations (data not shown) and all non-transplantation experimental analysis was performed in free-floating sections. For cryosectioning, brains were dissected and post-fixed in 4%PFA one hour at 4°C, then cryoprotected in 30% sucrose W/V in PBS overnight at 4°C. Prepared brains were mounted in Tissue-Tek (Takara) frozen at -80°C for storage until cryo-sectioned at -20°C in 12 µm sections for embryonic tissue and 20µm sections for adult tissue. Brains for cryosectioning were transcardially perfused as above and post-fixed in 4%PFA overnight at 4°C. Brains were embedded in 4% low melt agarose in PBS and sectioned to 50µm on a Leica VT1000S vibratome. Sections were stored in a propylene glycol:glycerol:PBS solution (3:3:4) at -20°C until used. For immunohistochemistry, cryosections were allowed to dry for 1-2 hours then frozen at -20°C until they were used. Frozen sections were defrosted and dried at room temperature for 1 hour then rehydrated in blocking solution (4% normal serum, 0.1% TritonX-100 in PBS) for 1-4 hours. Primary antibody incubation followed in blocking solution overnight at 4°C. Primary antibodies were

used at the following concentrations: Rat anti-SST (Millipore 1:500, [RRID:AB_2255374](#)), mouse monoclonal anti-Parvalbumin (Sigma 1:1000, [RRID:AB_477329](#)), Rabbit anti-VIP (Immunostar 1:1000, [RRID:AB_572270](#)), Mouse anti-CR50 (MBL, 1:1000, [RRID:AB_843523](#)). Sections were washed repeatedly in PBS then incubated in secondary antibodies conjugated to Alexafluor 488, 594, or 647, host matching serum used for blocking, for 45 minutes at room temperature. Free-floating sections were incubated in blocking solution (10% serum, 0.3% TritonX-100 in PBS) overnight at 4°C then incubated in primary antibody overnight at 4°C using the antibodies listed above. Free-floating washing steps in PBS were performed overnight or for 4 hours at room temperature. When nuclear labeling was desired, DAPI was applied after secondary antibody at 1:10,000 in PBS for 5 minutes. Slides (free-floating and cryosectioned) were promptly mounted with Fluoromount-G (Southern Biotech) and coverslipped.

***In situ* Hybridization**—Cryosectioned embryonic tissue was prepared for *in situ* hybridization using RNAScope (ACDbiosystems). Protocol was performed using probes for Ryk, Wnt7b, and TCF7L2 as described for Multiplex Fluorescent v2. Tissue permeabilization was achieved through application of Protease III for 30 minutes.

Ultrasound guided *in utero* transplantation—Ultrasound guided *in utero* transplantation was performed as previously described except where noted below (Au et al., 2013; Liu et al., 1998; Nery et al., 2002; Wichterle et al., 2001). For transplantation of β -catenin mutant, plugs were generated from a cross of *Nkx2.1^{Cre}*; β -catenin^{f+} males with β -catenin^{fl/fl}; *RCE^{fl/fl}* females. Homozygous mutant embryos were identified after dissection by midline fusion at the base of the MGE, and tissue samples from the embryo were retained for post-hoc genotyping confirmation. Mutant MGE's were dissected and pooled for transplants as above. Ryk^{-/-} embryos could not be identified visually, so pregnant females were deeply anesthetized, and the uterus gently cut to reveal the amniotic sacs. Tail samples were carefully removed from each embryo and rapidly processed for PCR genotyping (as described (Halford et al., 2000)), leaving the embryos in place. MGEs were dissected from the identified mutant embryos and processed for transplantation. E13.5 wild-type, unlabeled MGE or LGE tissue was mixed with mutant MGE and used as carrier when little mutant tissue (2 MGEs-1 null embryo) was available for transplantation.

***In utero* injections and electroporation**—Timed pregnant Swiss Webster females were deeply anesthetized with isoflurane and an incision was made to expose the uterus. IWP2 (sigma) dissolved in DMSO according to manufacturer guidelines, cyclopamine (CalBioChem) was dissolved in ethanol according to manufacturer guidelines, or antibody solution was frontloaded into a beveled glass pipette (as above). 25 nl of IWP2, 50nl of cyclopamine or 100 nl of function-blocking antibody were injected into the ventricles of e12.5 Swiss Webster embryos, the uterus was replaced and the incision stitched, allowing the pups to be born normally or sacrificed 1 day later for MGE collection and transplantation or analysis. Appropriate diluent without chemical was injected as a control. Animals for IWP2 treatment and transplantation experiments were Ai9-germline recombined, wildtype animals were used for function-blocking experiments. Cyclopamine injections were performed on all embryos resultant of *Nkx2.1^{Cre}*; *Ryk^{fl/+}* and *Ryk^{fl/+}* crosses. *In utero*

electroporation of the MGE was performed as previously described (Petros et al., 2015). The conditional *Ryk ICD* construct for electroporation was generated as described below (Cell culture) and subcloned downstream of a Nestin promoter and a floxed stop cassette to limit overexpression to the progenitor phase. To allow for post-hoc identification a pCAG driven GFP downstream of a floxed stop cassette was co-electroporated, or electroporated alone as control.

Rostral/caudal MGE dissections—Animals expressing a ubiquitous fluorescent marker were generated by crossing either *Ai9* (Madisen et al., 2010) or *RCE* (Sousa et al., 2009) reporter mice with the germline *Cre* driver *TK^{Cre}* (Bai et al., 2002). Pilot experiments were performed using unlabeled SW embryos, dissected MGEs were labeled using a PKH26 Red Fluorescent Cell Linker Mini Kit for General Cell Membrane Labeling (Sigma) following manufacturer's instructions. Ubiquitous fluorescent males were crossed with SW females, and pregnant females were collected at e12.5, morning of vaginal plug discovery counted as e0.5. Embryos were collected and brains were dissected into ice-cold PBS. Cortices were removed and rostral MGE or cMGE was dissected and treated as previously described (Butt et al., 2005). 10-20 embryos were collected and pooled for each condition.

Wnt signaling reporter fate-mapping—Transgenic embryos from timed pregnant *Tcf/Lef::H2b-dGFP*; pan *Ai9+* females were identified under a fluorescent microscope. *Ai9* positive, eGFP negative MGEs and positive MGEs were collected and processed for FACS sorting (Supplemental Figure 3). Negative MGEs were used for gating. eGFP; *Ai9* positive MGEs were dissociated and prepared for FACS sorting following normal cell dissociation methods used for transplantation as described above. Cells were sorted according to expression of eGFP using an iCyt reflection sorter with a 100uM nozzle by the NYU Cytometry and Cell sorting core facility (supported by Perlmutter Cancer Center grant P30CA016087). Collected cells (approximately 9% of cells sorted) were then transplanted into e13 embryos as above.

Quantification and statistical analysis—Transplanted cells in cortical areas from sections containing the hippocampus were identified by their expression of the appropriate ubiquitous label (PKH, eGFP or TdTomato) and assessed for their co-expression of SST or PV. Cells were categorized as SST+, PV+ or 'unidentified' (no marker or co-expression of both markers). A minimum of 200 cells were counted per brain, from areas distributed across multiple anterior-posterior sections. Ratios of PV or SST were calculated out of 'unidentified' cells (PV+ or SST+). Ratios in each brain are reported as a single n, and compared across conditions in GraphPad prism software through un-paired student's t-test or Chi-squared test as noted. In cases where reporter expression was not available (cyclopamine experiments), stained 50uM sections were imaged at 40x using a tiling microscope and absolute numbers of stained cells were counted for a standardized volume spanning all cortical layers.

Data and Code availability—The published article includes all datasets generated and analyzed during this study.

Supplementary Material

Refer to Web version on PubMed Central for supplementary material.

Acknowledgements

The authors wish to thank Kat Hadjantonakis and Wange Lu for generous donation of Tcf/Lef:H2B-dGFP and *Ryk*^{-/-} animals, respectively. Andre Goffinet for guidance on *Vangl2* mutants. Dhananjay Bambah-Mukku and Marian Fernandez Otero of the Dulac and Fishell laboratories, respectively for RNAscope protocol advice and reagents. Zhimin Lao and Alexandra Joyner for helpful discussions about Shh signaling and performing Gli1 in situ hybridization. This work was supported by the following NIH grants: F30 MH087045 (MGM), T32 MH015174-40 (MGM), R01-NS081297 (GF), R01-MH071679 (GF), P01-NS074972 (GF), and generous support from the Simons Foundation (GF) and the Whitehall Foundation (EA). M.G.M was supported by the NYU Medical Scientist Training Program.

References

- Anderson SA, Eisenstat DD, Shi L, and Rubenstein JL (1997). Interneuron migration from basal forebrain to neocortex: dependence on *Dlx* genes. *Science* 278, 474–476. [PubMed: 9334308]
- Au E, Ahmed T, Karayannis T, Biswas S, Gan L, and Fishell G (2013). A modular gain-of-function approach to generate cortical interneuron subtypes from ES cells. *Neuron* 80, 1145–1158. [PubMed: 24314726]
- Bai CB, Auerbach W, Lee JS, Stephen D, and Joyner AL (2002). Gli2, but not Gli1, is required for initial Shh signaling and ectopic activation of the Shh pathway. *Development* 129, 4753–4761. [PubMed: 12361967]
- Barrott JJ, Cash GM, Smith AP, Barrow JR, and Murtaugh LC (2011). Deletion of mouse *Porcn* blocks Wnt ligand secretion and reveals an ectodermal etiology of human focal dermal hypoplasia/Goltz syndrome. *Proc Natl Acad Sci U S A* 108, 12752–12757. [PubMed: 21768372]
- Brault V, Moore R, Kutsch S, Ishibashi M, Rowitch DH, McMahon AP, Sommer L, Boussadia O, and Kemler R (2001). Inactivation of the beta-catenin gene by Wnt1-Cre-mediated deletion results in dramatic brain malformation and failure of craniofacial development. *Development* 128, 1253–1264. [PubMed: 11262227]
- Briscoe J, and Ericson J (2001). Specification of neuronal fates in the ventral neural tube. *Curr Opin Neurobiol* 11, 43–49. [PubMed: 11179871]
- Butt SJ, Fuccillo M, Nery S, Noctor S, Kriegstein A, Corbin JG, and Fishell G (2005). The temporal and spatial origins of cortical interneurons predict their physiological subtype. *Neuron* 48, 591–604. [PubMed: 16301176]
- Cadigan KM, and Waterman ML (2012). TCF/LEFs and Wnt signaling in the nucleus *Cold Spring Harb Perspect Biol* 4.
- Cardin JA, Carlen M, Meletis K, Knoblich U, Zhang F, Deisseroth K, Tsai LH, and Moore CI (2009). Driving fast-spiking cells induces gamma rhythm and controls sensory responses. *Nature* 459, 663–667. [PubMed: 19396156]
- Chang WH, Choi SH, Moon BS, Cai M, Lyu J, Bai J, Gao F, Hajjali I, Zhao Z, Campbell DB, et al. (2017). Smek^{1/2} is a nuclear chaperone and cofactor for cleaved Wnt receptor Ryk, regulating cortical neurogenesis *Proc Natl Acad Sci U S A*.
- Charron F, and Tessier-Lavigne M (2005). Novel brain wiring functions for classical morphogens: a role as graded positional cues in axon guidance. *Development* 132, 2251–2262. [PubMed: 15857918]
- Chen B, Dodge ME, Tang W, Lu J, Ma Z, Fan CW, Wei S, Hao W, Kilgore J, Williams NS, et al. (2009). Small molecule-mediated disruption of Wnt-dependent signaling in tissue regeneration and cancer. *Nat Chem Biol* 5, 100–107. [PubMed: 19125156]
- De Marco Garcia NV, Karayannis T, and Fishell G (2011). Neuronal activity is required for the development of specific cortical interneuron subtypes. *Nature* 472, 351–355. [PubMed: 21460837]

- De Marco Garcia NV, Priya R, Tuncdemir SN, Fishell G, and Karayannis T (2015). Sensory inputs control the integration of neurogliaform interneurons into cortical circuits. *Nat Neurosci* 18, 393–401. [PubMed: 25664912]
- Dehorter N, Ciceri G, Bartolini G, Lim L, del Pino I, and Marin O (2015). Tuning of fast-spiking interneuron properties by an activity-dependent transcriptional switch. *Science* 349, 1216–1220. [PubMed: 26359400]
- Dessaud E, Yang LL, Hill K, Cox B, Ulloa F, Ribeiro A, Mynett A, Novitsch BG, and Briscoe J (2007). Interpretation of the sonic hedgehog morphogen gradient by a temporal adaptation mechanism. *Nature* 450, 717–720. [PubMed: 18046410]
- Ericson J, Briscoe J, Rashbass P, van Heyningen V, and Jessell TM (1997). Graded sonic hedgehog signaling and the specification of cell fate in the ventral neural tube. *Cold Spring Harb Symp Quant Biol* 62, 451–466. [PubMed: 9598380]
- Ferrer-Vaquer A, Piliszek A, Tian G, Aho RJ, Dufort D, and Hadjantonakis AK (2010). A sensitive and bright single-cell resolution live imaging reporter of Wnt/ss-catenin signaling in the mouse. *BMC Dev Biol* 10, 121. [PubMed: 21176145]
- Fino E, and Yuste R (2011). Dense inhibitory connectivity in neocortex. *Neuron* 69, 1188–1203. [PubMed: 21435562]
- Fishell G, and Rudy B (2011). Mechanisms of inhibition within the telencephalon: “where the wild things are”. *Annu Rev Neurosci* 34, 535–567. [PubMed: 21469958]
- Flames N, Pla R, Gelman DM, Rubenstein JL, Puelles L, and Marin O (2007). Delineation of multiple subpallial progenitor domains by the combinatorial expression of transcriptional codes. *J Neurosci* 27, 9682–9695. [PubMed: 17804629]
- Glickstein SB, Moore H, Slowinska B, Racchumi J, Suh M, Chuhma N, and Ross ME (2007). Selective cortical interneuron and GABA deficits in cyclin D2-null mice. *Development* 134, 4083–4093. [PubMed: 17965053]
- Green J, Nusse R, and van Amerongen R (2014). The role of Ryk and Ror receptor tyrosine kinases in Wnt signal transduction. *Cold Spring Harb Perspect Biol* 6.
- Gulacsi AA, and Anderson SA (2008). Beta-catenin-mediated Wnt signaling regulates neurogenesis in the ventral telencephalon. *Nat Neurosci* 11, 1383–1391. [PubMed: 18997789]
- Halford MM, Macheda ML, Parish CL, Takano EA, Fox S, Layton D, Nice E, and Stacker SA (2013). A fully human inhibitory monoclonal antibody to the Wnt receptor RYK. *PLoS One* 8, e75447. [PubMed: 24058687]
- Hollis ER 2nd, Ishiko N, Yu T, Lu CC, Haimovich A, Tolentino K, Richman A, Tury A, Wang SH, Pessian M, et al. (2016). Ryk controls remapping of motor cortex during functional recovery after spinal cord injury. *Nat Neurosci* 19, 697–705. [PubMed: 27065364]
- Hu H, Gan J, and Jonas P (2014). Interneurons. Fast-spiking, parvalbumin(+) GABAergic interneurons: from cellular design to microcircuit function. *Science* 345, 1255263. [PubMed: 25082707]
- Hu JS, Vogt D, Lindtner S, Sandberg M, Silberberg SN, and Rubenstein JLR (2017). Coup-TF1 and Coup-TF2 control subtype and laminar identity of MGE-derived neocortical interneurons. *Development* 144, 2837–2851. [PubMed: 28694260]
- Inan M, Blazquez-Llorca L, Merchan-Perez A, Anderson SA, DeFelipe J, and Yuste R (2013). Dense and overlapping innervation of pyramidal neurons by chandelier cells. *J Neurosci* 33, 1907–1914. [PubMed: 23365230]
- Inan M, Welagen J, and Anderson SA (2012). Spatial and temporal bias in the mitotic origins of somatostatin- and parvalbumin-expressing interneuron subgroups and the chandelier subtype in the medial ganglionic eminence. *Cereb Cortex* 22, 820–827. [PubMed: 21693785]
- Kamitori K, Tanaka M, Okuno-Hirasawa T, and Kohsaka S (2005). Receptor related to tyrosine kinase RYK regulates cell migration during cortical development. *Biochem Biophys Res Commun* 330, 446–453. [PubMed: 15796903]
- Kepecs A, and Fishell G (2014). Interneuron cell types are fit to function. *Nature* 505, 318–326. [PubMed: 24429630]

- Kvitsiani D, Ranade S, Hangya B, Taniguchi H, Huang JZ, and Kepecs A (2013). Distinct behavioural and network correlates of two interneuron types in prefrontal cortex. *Nature* 498, 363–366. [PubMed: 23708967]
- Lanoue V, Langford M, White A, Sempert K, Fogg L, and Cooper HM (2017). The Wnt receptor Ryk is a negative regulator of mammalian dendrite morphogenesis. *Sci Rep* 7, 5965. [PubMed: 28729735]
- Lapray D, Lasztocki B, Lagler M, Viney TJ, Katona L, Valenti O, Hartwich K, Borhegyi Z, Somogyi P, and Klausberger T (2012). Behavior-dependent specialization of identified hippocampal interneurons. *Nat Neurosci* 15, 1265–1271.
- Lee KJ, and Jessell TM (1999). The specification of dorsal cell fates in the vertebrate central nervous system. *Annu Rev Neurosci* 22, 261–294. [PubMed: 10202540]
- Lovett-Barron M, Turi GF, Kaifosh P, Lee PH, Bolze F, Sun XH, Nicoud JF, Zemelman BV, Sternson SM, and Losonczy A (2012). Regulation of neuronal input transformations by tunable dendritic inhibition. *Nat Neurosci* 15, 423–430, S421–423. [PubMed: 22246433]
- Lyu J, Yamamoto V, and Lu W (2008). Cleavage of the Wnt receptor Ryk regulates neuronal differentiation during cortical neurogenesis. *Dev Cell* 15, 773–780. [PubMed: 19000841]
- Macheda ML, Sun WW, Kugathasan K, Hogan BM, Bower NI, Halford MM, Zhang YF, Jacques BE, Lieschke GJ, Dabdoub A, et al. (2012). The Wnt receptor Ryk plays a role in mammalian planar cell polarity signaling. *J Biol Chem* 287, 29312–29323. [PubMed: 22773843]
- Madisen L, Zwingman TA, Sunkin SM, Oh SW, Zariwala HA, Gu H, Ng LL, Palmiter RD, Hawrylycz MJ, Jones AR, et al. (2010). A robust and high-throughput Cre reporting and characterization system for the whole mouse brain. *Nat Neurosci* 13, 133–140. [PubMed: 20023653]
- Miyoshi G, Butt SJ, Takebayashi H, and Fishell G (2007). Physiologically distinct temporal cohorts of cortical interneurons arise from telencephalic Olig2-expressing precursors. *J Neurosci* 27, 7786–7798. [PubMed: 17634372]
- Nery S, Fishell G, and Corbin JG (2002). The caudal ganglionic eminence is a source of distinct cortical and subcortical cell populations. *Nat Neurosci* 5, 1279–1287. [PubMed: 12411960]
- Nusslein-Volhard C, and Wieschaus E (1980). Mutations affecting segment number and polarity in *Drosophila*. *Nature* 287, 795–801. [PubMed: 6776413]
- Petrossian TJ, Bultje RS, Ross ME, Fishell G, and Anderson SA (2015). Apical versus Basal Neurogenesis Directs Cortical Interneuron Subclass Fate. *Cell Rep* 13, 1090–1095. [PubMed: 26526999]
- Placzek M, Dodd J, and Jessell TM (2000). Discussion point. The case for floor plate induction by the notochord. *Curr Opin Neurobiol* 10, 15–22. [PubMed: 10679441]
- Proffitt KD, and Virshup DM (2012). Precise regulation of porcupine activity is required for physiological Wnt signaling. *J Biol Chem* 287, 34167–34178. [PubMed: 22888000]
- Puelles L, and Rubenstein JL (2003). Forebrain gene expression domains and the evolving prosomeric model. *Trends Neurosci* 26, 469–476. [PubMed: 12948657]
- Qu Y, Huang Y, Feng J, Alvarez-Bolado G, Grove EA, Yang Y, Tissir F, Zhou L, and Goffinet AM (2014). Genetic evidence that Celsr3 and Celsr2, together with Fzd3, regulate forebrain wiring in a Vangl-independent manner. *Proc Natl Acad Sci U S A* 111, E2996–3004. [PubMed: 25002511]
- Reynaud E, Lahaye LL, Boulanger A, Petrova IM, Marquilly C, Flandre A, Martinez T, Privat M, Noordermeer JN, Fradkin LG, et al. (2015). Guidance of *Drosophila* Mushroom Body Axons Depends upon DRL-Wnt Receptor Cleavage in the Brain Dorsomedial Lineage Precursors. *Cell Rep* 11, 1293–1304. [PubMed: 25981040]
- Roelink H, Porter JA, Chiang C, Tanabe Y, Chang DT, Beachy PA, and Jessell TM (1995). Floor plate and motor neuron induction by different concentrations of the amino-terminal cleavage product of sonic hedgehog autoproteolysis. *Cell* 81, 445–455. [PubMed: 7736596]
- Rubenstein JL, Martinez S, Shimamura K, and Puelles L (1994). The embryonic vertebrate forebrain: the prosomeric model. *Science* 266, 578–580. [PubMed: 7939711]
- Schmitt AM, Shi J, Wolf AM, Lu CC, King LA, and Zou Y (2006). Wnt-Ryk signalling mediates medial-lateral retinotectal topographic mapping. *Nature* 439, 31–37. [PubMed: 16280981]
- Sousa VH, Miyoshi G, Hjerling-Leffler J, Karayannis T, and Fishell G (2009). Characterization of Nkx6-2-derived neocortical interneuron lineages. *Cereb Cortex* 19 Suppl 1, i1–10.

- Sussel L, Marin O, Kimura S, and Rubenstein JL (1999). Loss of Nkx2.1 homeobox gene function results in a ventral to dorsal molecular respecification within the basal telencephalon: evidence for a transformation of the pallidum into the striatum. *Development* 126, 3359–3370. [PubMed: 10393115]
- Taniguchi H, Lu J, and Huang ZJ (2013). The spatial and temporal origin of chandelier cells in mouse neocortex. *Science* 339, 70–74. [PubMed: 23180771]
- Tyson JA, Goldberg EM, Maroof AM, Xu Q, Petros TJ, and Anderson SA (2015). Duration of culture and sonic hedgehog signaling differentially specify PV versus SST cortical interneuron fates from embryonic stem cells. *Development* 142, 1267–1278. [PubMed: 25804737]
- Wamsley B, and Fishell G (2017). Genetic and activity-dependent mechanisms underlying interneuron diversity. *Nat Rev Neurosci* 18, 299–309. [PubMed: 28381833]
- Wichterle H, Turnbull DH, Nery S, Fishell G, and Alvarez-Buylla A (2001). In utero fate mapping reveals distinct migratory pathways and fates of neurons born in the mammalian basal forebrain. *Development* 128, 3759–3771. [PubMed: 11585802]
- Willert K, Brown JD, Danenberg E, Duncan AW, Weissman IL, Reya T, Yates JR 3rd, and Nusse R (2003). Wnt proteins are lipid-modified and can act as stem cell growth factors. *Nature* 423, 448–452. [PubMed: 12717451]
- Willert K, and Nusse R (2012). Wnt proteins. *Cold Spring Harb Perspect Biol* 4, a007864. [PubMed: 22952392]
- Wonders CP, and Anderson SA. (2006). The origin and specification of cortical interneurons. *Nat Rev Neurosci* 7, 687–696. [PubMed: 16883309]
- Wonders CP, Taylor L, Welagen J, Mbata IC, Xiang JZ, and Anderson SA (2008). A spatial bias for the origins of interneuron subgroups within the medial ganglionic eminence. *Dev Biol* 314, 127–136. [PubMed: 18155689]
- Xu Q, Guo L, Moore H, Waclaw RR, Campbell K, and Anderson SA (2010). Sonic hedgehog signaling confers ventral telencephalic progenitors with distinct cortical interneuron fates. *Neuron* 65, 328–340. [PubMed: 20159447]
- Xu Q, Tam M, and Anderson SA (2008). Fate mapping Nkx2.1-lineage cells in the mouse telencephalon. *J Comp Neurol* 506, 16–29. [PubMed: 17990269]
- Xu Q, Wonders CP, and Anderson SA (2005). Sonic hedgehog maintains the identity of cortical interneuron progenitors in the ventral telencephalon. *Development* 132, 4987–4998. [PubMed: 16221724]
- Zhong J, Kim HT, Lyu J, Yoshikawa K, Nakafuku M, and Lu W (2011). The Wnt receptor Ryk controls specification of GABAergic neurons versus oligodendrocytes during telencephalon development. *Development* 138, 409–419. [PubMed: 21205786]

Highlights:

- Rostral and caudal subdomains of the MGE differentially produce PV and SST interneurons
- Wnt/Ryk signaling is required to establish MGE subdomains
- Ryk genetic loss of function results in gross misspecification of cortical interneurons
- In vitro activation of the Ryk pathway regulates ES differentiation to PV and SST cells

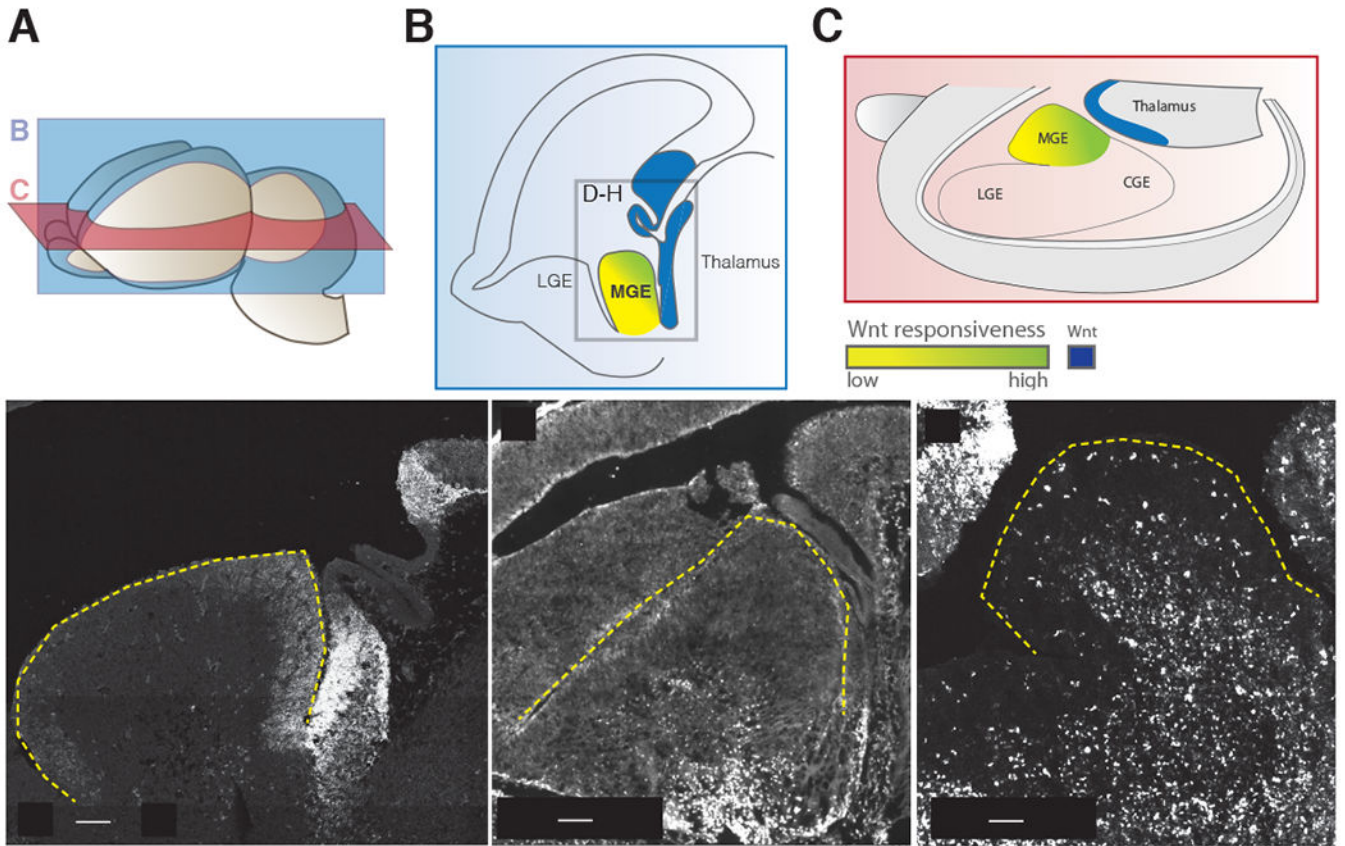


Figure 1. Expression of Wnt signaling factors present near the medial ganglionic eminence at embryonic day 13.5.

(A) Planes of section for (B) and (C) in relation to a whole e13.5 brain. (B) Parasagittal schematic of e13.5 caudal Wnt sources and Wnt responsiveness across the MGE. Box denotes cropped region for *in situ* hybridization images in D-H. (C) Schematic diagram in the transverse plane showing the same spatial relationship of caudal Wnt sources and Wnt responsiveness across the MGE. (D) *In situ* hybridization of Wnt7b, (E) TCF7L2 immuno staining for TCF7L2 protein, an early read-out for canonical Wnt signaling. TCF7L2 positive cells in the mantle are enriched in the caudal portion of the MGE. (F) Horizontal section of MGE in Tcf/Lef:H2B-dGFP reporter animals at 13.5, eGFP expression is enriched in the caudal MGE. The outline of the MGE is denoted by the yellow dashed line.

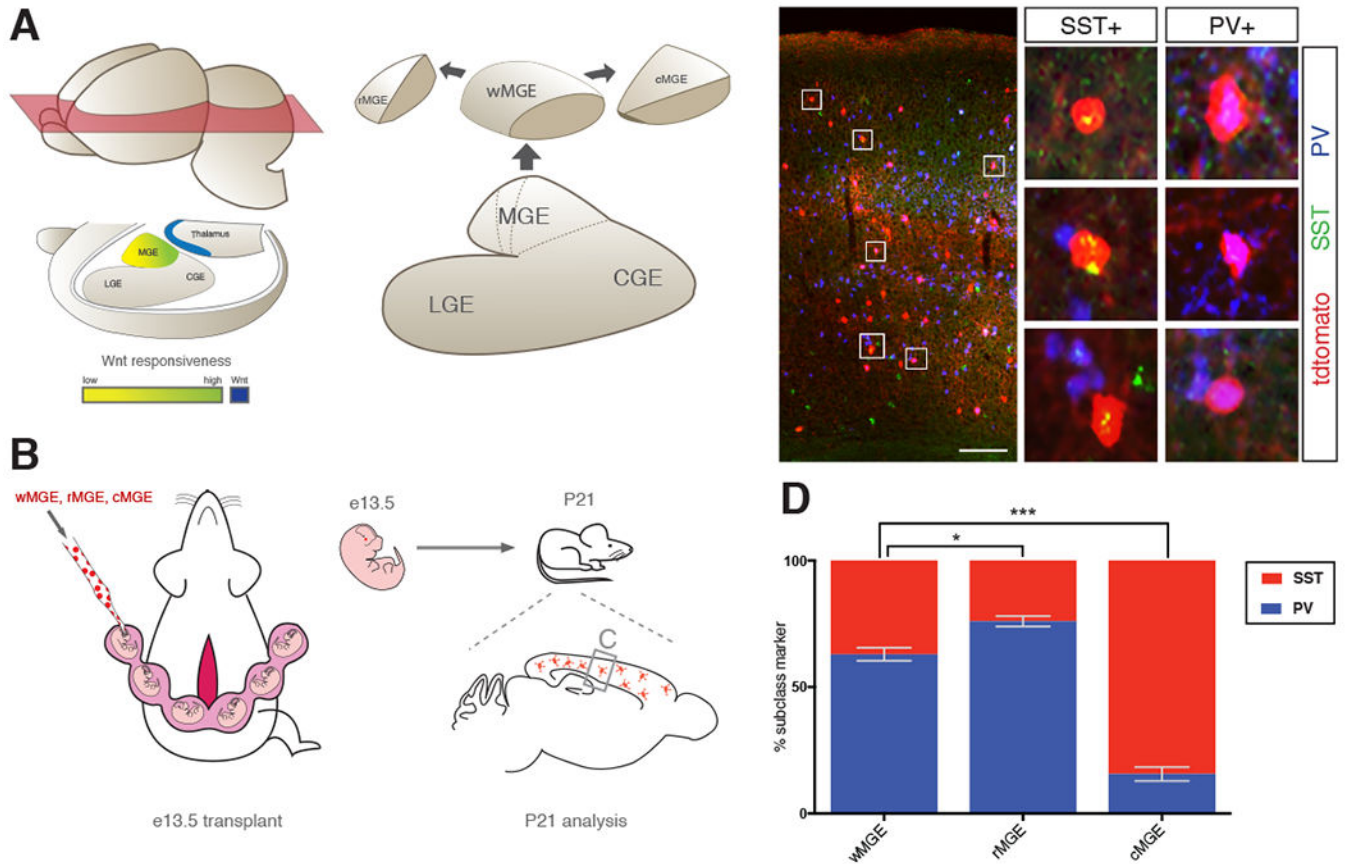


Figure 2. Ultrasound-guided in utero transplantation to determine the cortical interneuron output of MGE subdomains.

(A) Schematic diagram of spatial relationship between Wnt source (blue) and Wnt responsiveness within the MGE (green-to-yellow) suggests the presence of MGE subdomains along the rostral caudal axis. Whole (wMGE), rostral (rMGE) and caudal (cMGE) were dissected for transplantation studies. (B) Schematic of transplantation experiment. Pan-RFP expressing w-, r- and cMGE were transplanted into e13.5 mouse MGE in separate experiments by ultrasound backscatter microscopy. Host mice were sacrificed 27 days post transplant (postnatal day 21, P21) and donor cortical interneurons were analyzed for SST+ and PV+ expression. (C) Representative coronal section of P21 host forebrain showing RFP+ donor cells engrafted in cortex (scale bar 200um). Middle panel is higher magnification of box on left, boxes 1-6 show high power images of transplanted cells positive for RFP and either SST or PV. (D) P21 analysis of w-, r-, and cMGE transplantation studies for SST+ and PV+ expression in transplanted interneurons. Error bars standard error of the mean (* denotes $p < 0.05$; ** denotes $p < 0.01$; *** denotes $p < 0.001$).

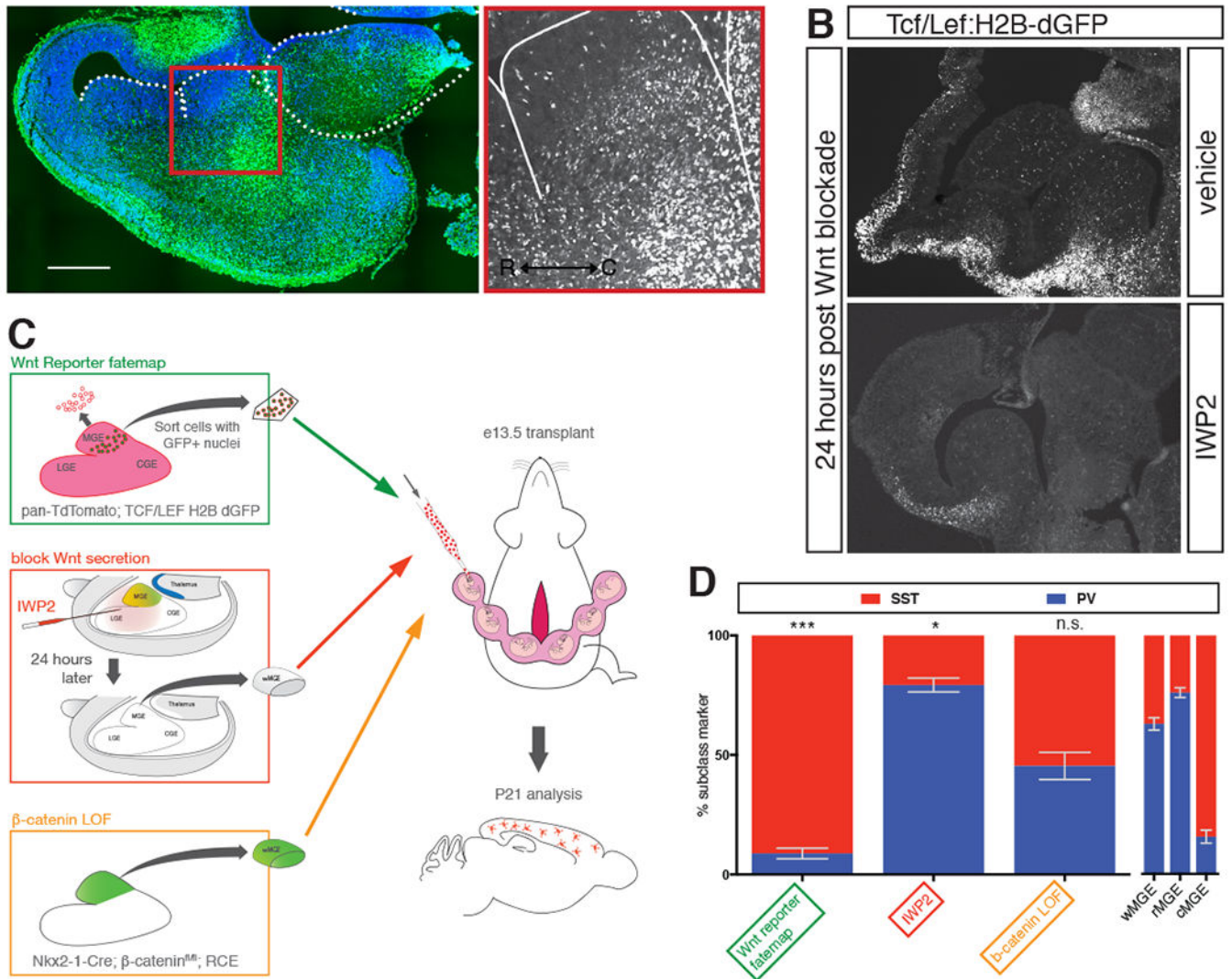


Figure 3. Exploring the role of Wnt signaling in determining cortical interneuron subtype identity.

(A) Transverse section of e13.5 mouse brain in Tcf/Lef:H2B-dGFP reporter mouse. Nuclear GFP is enriched in caudal portion of MGE. (B) Parasagittal section of Tcf/Lef:H2B-dGFP reporter mouse at e13.5 showing regions of Wnt-responsiveness. 24 hours after intraventricular injection of vehicle did not affect GFP signal. 24 hours following intraventricular injection of IWP2 strongly reduced GFP signal. (C) Schematic diagram depicting the different transplant studies performed to examine the role of Wnt in interneuron specification. Green box shows pan-RFP+ cells sorted for eGFP+ nuclei indicative of Wnt responsiveness. Red box shows intraventricular injection of IWP2 at e12.5, followed by dissection and transplant of wMGE 24 hours post-injection. Orange box shows genetic removal of β -catenin and simultaneous eGFP+ fate mapping of MGE prior to dissection and transplantation. (D) P21 analysis of studies transplanting Tcf/Lef:H2B-dGFP + MGE cells, blocking Wnt secretion prior to transplantation, or genetic removal of β -catenin in transplanted MGE. W-, r- and cMGE transplant results on right for comparison.

Error bars standard error of the mean (* denotes $p < 0.05$; ** denotes $p < 0.01$; *** denotes $p < 0.001$).

Author Manuscript

Author Manuscript

Author Manuscript

Author Manuscript

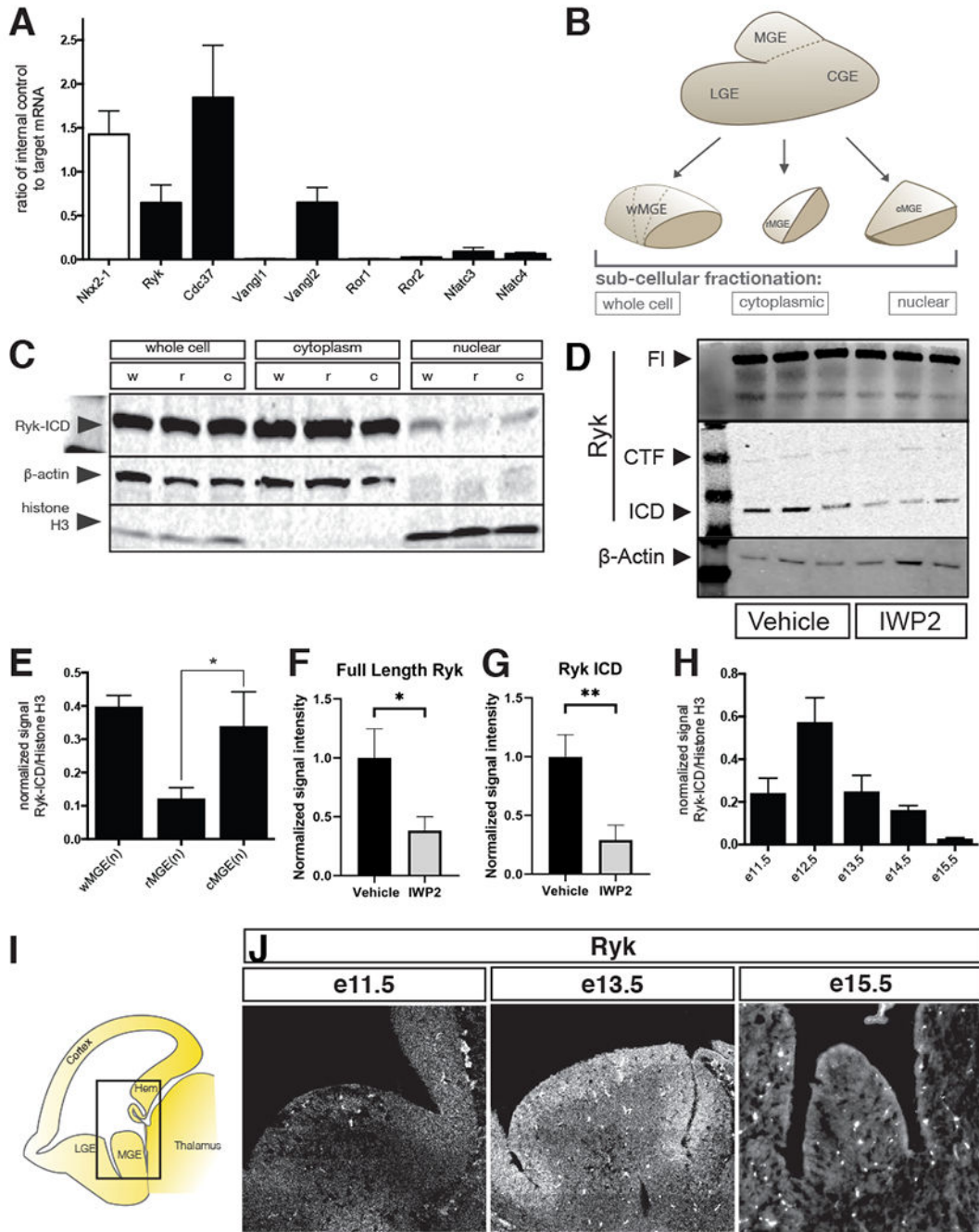


Figure 4. Identifying components of non-canonical Wnt and Ryk signaling in the embryonic MGE.

(A) Quantitative PCR of e12.5 MGE for non-canonical Wnt signaling components, Nkx2-1 shown as a positive control. (B) Schematic depiction of various MGE samples loaded for western blot in C. See also Supplemental figure 3. (C) Biochemical fractionations of w-, r- and cMGE into whole cell, cytoplasmic and nuclear components were analyzed by Western blot for Ryk, b-actin and histone H3 (latter two act as loading controls). (D) FL Ryk and Ryk ICD fragments are decreased in the cytoplasm of MGE cells 24hrs after IWP2 treatment. (E) Quantitation of blot in C: nuclear Ryk intracellular domain (Ryk-ICD) present

in w-, r- and cMGE samples. (F,G) Quantification of blot shown in D, normalized to loading control and average signal intensity of the vehicle treated bands. (H) wMGE nuclear fractions at various embryonic time points showing that Ryk signaling is dynamic over time. (I) Schematic of parasagittal sections of 13.5 mouse brain. Equivalent areas at e11.5, e13.5 and e15.5 show decreasing levels of Ryk receptor over developmental time by (J) *in situ* hybridization for Ryk.

Author Manuscript

Author Manuscript

Author Manuscript

Author Manuscript

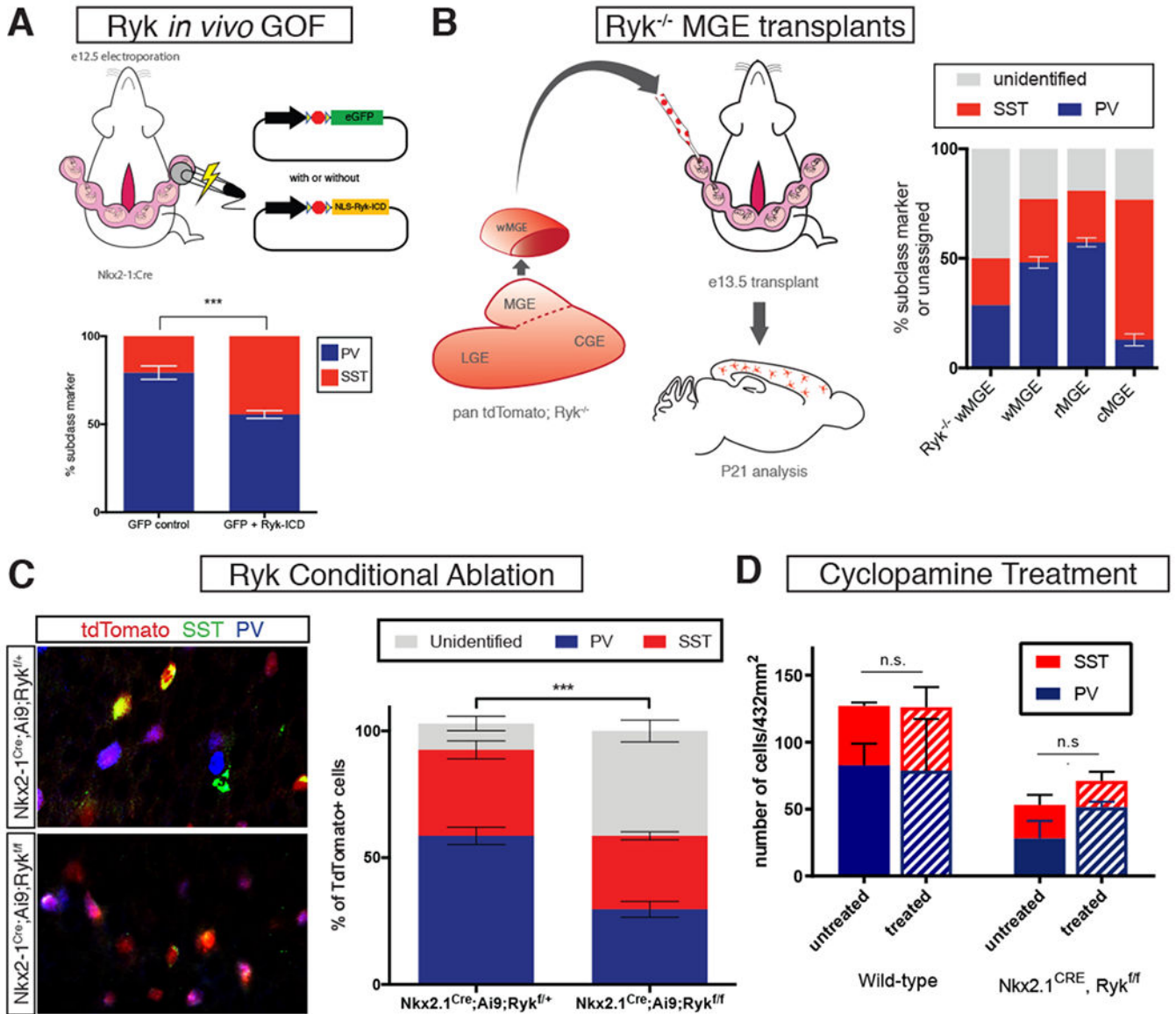


Figure 5. Ryk loss- and gain-of-function and its effects on cortical interneuron specification. (A) Left, schematic diagram of electroporation paradigm for Ryk ICD gain-of-function in MGE progenitors. Right, analysis of PV⁺ and SST⁺ interneurons at P21 with control (GFP alone) or Ryk ICD gain-of-function (NLS-Ryk-ICD) plasmid electroporation. Ryk-ICD GOF resulted in a significant increase in SST⁺ and a decrease in PV⁺ electroporated interneurons. (B) Schematic diagram showing *Ryk*^{-/-} MGE transplant study. (B) P21 analysis revealed that *Ryk*^{-/-} MGE transplants contain a large percentage of unidentified cortical interneurons; wild type w-, r-, and cMGE transplant results for comparison. (C) Conditional genetic ablation of *Ryk* and simultaneous labeling with tdTomato in the MGE using Nkx2-1^{Cre}. Left top, representative image of *Ryk*^{fl/fl}, left bottom, representative image of *Ryk*^{fl/fl}. tdTomato in red, somatostatin in green, parvalbumin in blue. Asterisks denote unidentified tdTomato⁺ cells. Right, quantification of unidentified, somatostatin⁺ and parvalbumin⁺ tdTomato⁺ cells for each group. Error bars standard error of the mean (*

denotes $p < 0.05$; ** denotes $p < 0.01$; *** denote $p < 0.001$). (D) Treatment of *Nkx2.1^{Cre}*, *Ryk^{f/f}* or WT embryos at e12.5 with cyclopamine has no significant nor additive effect on the numbers of PV+ and SST+ interneurons observed in adults.

Author Manuscript

Author Manuscript

Author Manuscript

Author Manuscript

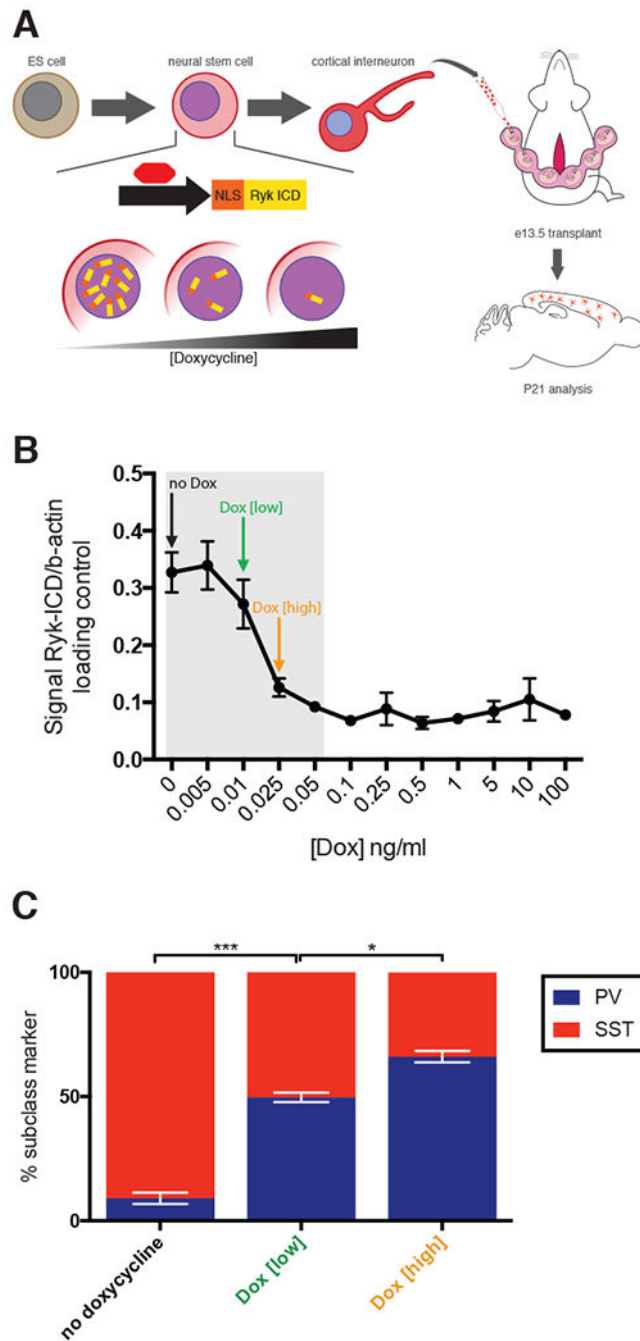


Figure 6. Investigating the role of graded Ryk signaling in interneuron lineage specification. (A) Schematic diagram of the regulation of tetracycline trans-activator, $tTA2^S$ by varying doxycycline added to medium during ES cell differentiation to interneuron. $tTA2^S$ activity regulates the graded expression of NLS-Ryk-ICD. After differentiation into interneurons, cells were transplanted by UBM at e13.5 and analyzed at P21 for SST⁺ and PV⁺ expression. (B) Doxycycline dose response curve was determined empirically in order to ascertain appropriate low and high doxycycline concentrations for transplant experiments. (C) Results of transplantation studies where ES cells were differentiated in no, low, or high doxycycline

concentrations. Error bars standard error of the mean (* denotes $p < 0.05$; ** denotes $p < 0.01$; *** denotes $p < 0.001$).

Author Manuscript

Author Manuscript

Author Manuscript

Author Manuscript

Key Resources Table

REAGENT or RESOURCE	SOURCE	IDENTIFIER
Antibodies		
Rat anti-SST	Millipore	Cat#MAB354 RRID:AB_2255374
mouse monoclonal anti-Parvalbumin	Sigma	Cat#P3088 RRID:AB_477329
Rabbit anti-VIP	Immunostar	Cat#20077 RRID:AB_572270
Mouse anti-CR50	MBL	Cat#D223-3 RRID:AB_843523
Rabbit monoclonal anti Ryk N-term	AbCam	RRID:AB_10973565
Rabbit anti-Ryk C-term	Thermo	RRID:AB_2285487
Rabbit anti-Ryk N-term	Hollis et al 2016	N/A
mouse anti Cyclophilin A	Abcam	RRID:AB_879767
Rb anti-histone H3	Cell Signaling	RRID:AB_331563
mouse anti β -actin	ThermoFisher	MA5-15739
Chemicals, Peptides, and Recombinant Proteins		
IWP2	sigma	Cat#686770-61-6
cyclopamine	CalBioChem	Cat#239803
Dkkopf-1	Tocris	Cat#5897-DK/CF
Sonic Hedgehog	Tocris	Cat#464-SH
Ryk function blocking antibody	Halford et al., 2013	N/A
Critical Commercial Assays		
RNAScope	ACDbiosystems	Cat#323100
Experimental Models: Cell Lines		
<i>Dlx6^{Cre}</i> ; Ai9	This paper	N/A
Experimental Models: Organisms/Strains		
<i>Nkx2-1^{Cre}</i>	Xu et al., 2008	JAX: 008661
<i>Ryk^{-/-}</i>	Halford et al., 2013	RRID:MGI:2667559
<i>β-catenin^{fl}</i>	Brault et al., 2001	JAX: 004152
<i>Tcf/Lef:H2B-dGFP</i>	Ferrer-Vaquer et al., 2010	(RRID:IMSR_JAX:013752)
<i>Ai9</i>	Madisen et al., 2010	equivalent: RRID:IMSR_JAX:007914
<i>RCE</i>	Sousa et al., 2009	JAX:32037
<i>TK^{Cre}</i>	Bai et al., 2002	MGI:4437924
<i>Ryk</i> conditional	Hollis et al., 2016	MGI:6147406
Oligonucleotides		
Ryk Primers		
Recombinant DNA		
Nestin-Nkx2-1-IRES-tTA	Au et al., 2013	N/A

REAGENT or RESOURCE	SOURCE	IDENTIFIER
Antibodies		
Dlx2 – TetO – NLS-RykICD	This paper	N/A
Nestin – LSL – NLS-RykICD	This paper	N/A
pCAG – LSL - eGFP	Petros et al., 2015	N/A

Author Manuscript

Author Manuscript

Author Manuscript

Author Manuscript